Journal of Fluids and Structures 86 (2019) 124–134

Contents lists available at ScienceDirect

Journal of Fluids and Structures

journal homepage: www.elsevier.com/locate/jfs

Curvature-based, time delayed feedback as a means for self-propelled swimming

David Gross [a,b], Yann Roux [a], Médéric Argentina [b,*]

[a] K-Epsilon S.A.R.L., 1300 Route des Cretes, 06560 Valbonne, France
[b] Université Côte d'Azur, CNRS, INPHYNI, France

ARTICLE INFO

Article history:
Received 10 August 2018
Received in revised form 4 December 2018
Accepted 23 January 2019
Available online xxxx

Keywords:
Swimming
Muscle activation
Proprioception
Vortex panel

ABSTRACT

The development of bio-inspired robotics has led to an increasing need to understand the strongly coupled fluid–structure and control problem presented by swimming. Usually, the mechanical forcing of muscles is modeled with an imposed distribution of bending moments along the swimmer's body. A simple way to exploit this idea is to define a central pattern forcing for this active driving, but this approach is not completely satisfactory because locomotion results from the interaction of the organism and its surroundings. Gazzola et al. (2015) have proposed that a curvature-based feedback with a time delay can trigger self-propulsion for a swimmer without necessitating such a pre-defined forcing. In the present work, we implement this feedback within a numerical model. We represent the swimmer as a thin elastic beam using a finite element representation which is coupled to an unsteady boundary element method for the resolution of the fluid domain. The model is first benchmarked on a flexible foil in forced leading edge heave.

To recover previous findings, an imposed traveling bending moment wave is then used to drive the swimmer which yields peaks in the mean forward velocity when the driving frequency corresponds to the natural frequencies of the elastic structure. Delayed, curvature-based feedback is then applied to the swimmer and produces peaks in the velocity for delays that differ from the natural periods, associated to its deformations modes. Finally, a simplified model is shown to qualitatively describe the origin of the peaks observed in the feedback swimmer.

1. Introduction

The subject of swimming propulsion by means of body undulations has been the subject of considerable research. With the advent of bio-inspired robotics as an alternative to traditionally propelled robots, there is an ever increasing need to understand both the strongly coupled fluid–structure interaction and control problem associated with swimming.

Theoretical mechanisms of swimming embraces many aspects of propulsion. In the asymptotic limit of a very slender swimmer, Lighthill's elongated-body theory (EBT) (Lighthill, 1960) has seen considerable use and extension (Candelier et al., 2011; Eloy et al., 2010; Yu and Eloy, 2018). Lighthill initially developed EBT based on the slender body theory of Munk (1924). This approach is based on the independence of the potential flow about a transverse section of the body from that of it neighboring sections. Lighthill later used momentum balancing arguments to extended EBT to large amplitudes (Lighthill, 1971). A well-known result of EBT is that thrust production is entirely dependent on the behavior of the tail (Lighthill, 1971).

* Corresponding author.
E-mail address: mederic.argentina@unice.fr (M. Argentina).

https://doi.org/10.1016/j.jfluidstructs.2019.01.023
0889-9746/

Likewise, the case of a 2D swimmer has seen much development since first investigated by Wu (1961, 2007). Numerical approaches have also been applied to understand particular aspects of propulsion. For example, the work of Carling et al. represented an early attempt to perform solved, self-propelled swimming with an imposed body deformation (Carling et al., 1998) which inspired numerous other authors (Leroyer and Visonneau, 2005; van Rees et al., 2013).

To answer whether fundamental mechanisms can be identified in swimming, we need to understand the selection process of gait kinematics. The work of Bainbridge (1958, 1960) was notable in identifying a number of trends in the gait parameters. Specifically, he noted that the swimming speed was linearly related to the tail beat amplitude, A, which itself appeared to increase up to a maximum of about $0.2L$, where L is the swimmer length (Bainbridge, 1958). Likewise, he recognized that for a given body length, the swimming speed was proportional to the tail beat frequency f (Bainbridge, 1958). Unfortunately, he did not try to rationalize these results to swimmers in general. For rainbow trouts, Webb and Kostecki found the that wavelength was independent of swimming speed, but varied with a power relation to the fish length and was relatively larger in small fish (Webb et al., 1984). As an attempt to capture the characteristics of fish swimming, Triantafyllou et al. introduced the use of Strouhal number, $St = fA/U$ (Triantafyllou et al., 1991, 1993), based on experiments with flapping foils. Notably, Triantafyllou et al. (2005) showed that for flapping foils an optimum in efficiency is observed around a St of 0.25–0.35. By exploiting an extensive survey of swimming organisms, Gazzola et al. (2014) characterized the gait of swimmers based on whether they are in the laminar or turbulent regime. In this work, the authors balanced the propulsive force against the drag force. In the laminar regime, this was done exploiting the viscous drag of a Blasius flat plate and in the turbulent regime by balancing the thrust against a pressure drag. This rather simplistic approach was successful in predicting the swimming speed over seven orders of magnitude of the Reynolds number (Gazzola et al., 2014).

The subject of muscle activation has been the object of considerable research, from a biological perspective. The early work of Hill (1938) led to a simple mechanical model for describing muscles. The muscles receive impulses from a central nervous system, but their response may be regulated by a proprioceptive feedback signal generated by the stretch of the muscle itself (Shadmehr and Wise, 2005). The changes in muscle activation for different gaits were investigated by Wardle et al. (1995). They noted that all three of the species they examined exhibited negative work, whereby muscles are contributing to stiffen the body to better transmit power to the tail. To model the muscle action, Cheng et al. imposed bending moments on a beam representation of a swimmer with the hydrodynamics taken into account with 3D waving plate theory (Cheng et al., 1998). A complete 2D Navier–Stokes simulation of a lamprey modeled using springs (Tytell et al., 2010) has been developed to study the effects of variations of elastic bending stiffness, fluid density and muscle driving force. In this work, the kinematic behavior was found to have an optimum combination of muscle force and stiffness for maximizing steady speed or acceleration. For efficient locomotion, a coupling between the muscle activity and the sensing of the environment is necessary. Liao et al. showed experimentally that trouts could perceive the von Kármán sheet of an upstream obstacle and altered their gait to reduce their energy consumption (Liao et al., 2003). To reproduce a neuromechanical system, Ekeberg et al. (1995) developed simulations of a simplified lamprey neural network. In their model, they incorporated a mechanical feedback which modulated the central pattern and yielded realistic swimming motions. Gazzola et al. showed that a simple body curvature feedback model is sufficient to establish a swimming gait without the need for a central pattern generator (Gazzola et al., 2015). This approach could be exploited to alter the shape of the peaks in the performance. Such a proprioceptive mechanism might have biological implications. For example, lampreys are known to have specialized mechanoreceptors called edge cells along their spinal cords that respond to bending and modify the behavior of the central pattern generator (Guan et al., 2001).

In this work, a delayed, curvature-based feedback mechanism is numerically explored as a means to locomotion. We believe that feedback forcing is the first direction to take for giving autonomy to fish like vehicles, because the locomotion velocity will be adapted to the environment of the swimmer. Our approach follows the philosophy of the work Gazzola et al. (2015). In this article, the authors have used a simple model derived in Argentina and Mahadevan (2005) for predicting the pressure imposed on the swimmer. The dynamics of the swimmer is computed using a modal decomposition, which is useful to study the cruising regime of locomotion. Such a model is limited to small deformations of the body and restricted to swim in one dimension. In this manuscript, we relax these restrictions to permit non-stationary regimes and 2D motions of the fish. The influence of system damping and the feedback delay on the response is studied using a 2D swimmer modeled as an Euler–Bernoulli beam subjected to fluid forces computed from a boundary element approach. Details of the model are specified in the methodology section. The swimmer model is first validated by comparing its predictions to the experimental results of Paraz et al. (2014), Paraz (2015) and Paraz et al. (2016) in which a flexible sheet is given a periodic heaving motion at the leading edge. The behavior of a swimmer driven by a traveling bending moment wave, is then illustrated. The results of feedback locomotion are then presented and contrasted to self-propulsion induced by forced bending moments. Finally, a simple one degree of freedom model is shown to qualitatively describe the characteristics of the feedback swimmer.

2. Methodology

We wish to numerically solve the fluid–structure interaction problem associated with the 2D swimmer. The swimmer's form is defined by a curve depicting its spine (as shown in Fig. 1). The swimmer body is modeled by an Euler–Bernoulli beam. For the fluid part, we approximate the swimmer's boundaries with 20 panels whose end nodes are shared with the beam. A 2D, unsteady panel method with a vortex particle representation of the wake (Rehbach, 1973, 1978) is implemented to numerically solve the fluid problem.

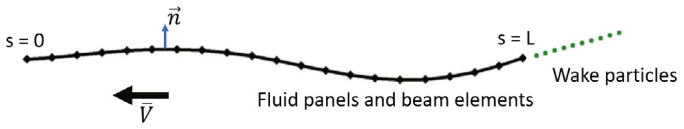

Fig. 1. The swimmer is modeled by an Euler–Bernoulli beam which is discretized into beam elements and fluid panels while its wake is represented with point vortices.

The panels are discretized using point vortices located at their extremities. The influence of these vortices is determined from the 2D Biot–Savart law:

$$u = \frac{\Gamma}{2\pi d} \tag{1}$$

where u is the magnitude of the induced velocity from a point vortex of strength Γ at a distance d from the location of interest.

Each panel's pair of vortices is equivalent to a constant strength dipole located at the panel midpoint (Katz and Plotkin, 2001). The non-penetration condition is enforced at the panel midpoint with a Neumann approach:

$$\boldsymbol{U}_n = \nabla\Phi \cdot \boldsymbol{n} = \boldsymbol{0} \tag{2}$$

where $\boldsymbol{U}_n$ is the normal velocity relative to the moving panel, Φ is the velocity potential and $\boldsymbol{n}$ is the panel's normal vector.

The general idea of panel methods is to determine the solution of a system of the form:

$$[A]\boldsymbol{\gamma} = \boldsymbol{b} \tag{3}$$

where $[A]$ is a matrix describing the influence of each panel on the others, $\boldsymbol{\gamma}$ is the strength of the singularity elements of the panels which are the unknowns to be solved, and $\boldsymbol{b}$ are the boundary conditions (2). Solving the above system requires the inversion of a dense matrix as all panels influence one another. $[A]$ is dependent on the current geometric form of the swimmer which changes over time. As the body deforms slowly, the influence matrix is expected to vary gradually; a Newton iterative method is used to invert $[A]$ using the prior inverse of $[A]$ as an initial guess (Pan and Reif, 1985; Pan and Schreiber, 1990).

The above inviscid approach is insufficient to generate lift and hence an additional constraint is required to properly develop the associated circulation. The Kutta condition achieves this by obliging the flow to leave the trailing edge smoothly. To enforce the unsteady Kutta condition, the vorticity of the trailing edge vertex is removed and transferred to the wake (Katz and Plotkin, 2001). As a discrete time stepping solution will be used, the continuous wake sheet is approximated by point-like vortices. This approach was originally developed by Rehbach (1973, 1978) and has seen applications since then for a number of unsteady aerodynamic problems (Huberson, 1984, 1986; Charvet, 1992; Hauville, 1996; Willis, 2006; Melli, 2008).

The swimmer which is both flexible and slender, is treated as an unconstrained, in-extensible Euler–Bernoulli beam of uniform mass m, stiffness EI, and length L, free to be largely deformed as described in Timoshenko and Woinowsky-Krieger (1959). The beam is discretized with a small-strain, large displacement, large rotation, co-rotational finite element formulation (Felippa and Haugen, 2005). In the present case, we model a structural damping with a Kelvin–Voigt model (Eldred et al., 1995; Banks and Inman, 1991), which is proportional to the strain rate. Although we solve the non-linear problem, for clarity, we present here, in the limit of small rotations and displacements, the swimmer's structural equation:

$$m\partial_{tt}y + \partial_{ss}(\eta EI\partial_{tss}y) + EI\partial_{ssss}y = F(s,t), \tag{4}$$

where m is the mass per unit length, y is the transverse deformation of the beam (i.e. perpendicular to the locomotion velocity), s is the arc-length position along the swimmer (see Fig. 1), η is a Kelvin–Voigt damping coefficient with units of seconds. The beam equation is treated with the non-linearities arising due to large rotations and displacement, but maintaining constant the bending stiffness and rotational inertia as the beam section is assumed to remain unchanged.

$F(s,t)$ is the sum of the input forces which will include the fluid forces as well as those resulting from imposed bending moments. We have used the unsteady Bernoulli relation for computing the fluid stresses as depicted in Katz and Plotkin (2001). The active part is imposed through a propagating wave or a local feedback. ηE has dimensions of Pa s, hence the Kelvin–Voigt damping models the viscosity of the structure. The swimmer is free at both ends; for the sake of clarity, we write the boundary conditions, in the small deformation limit:

$$\partial_{sss}y_{(s=0,L)} = 0 \qquad \partial_{ss}y_{(s=0,L)} = 0, \tag{5}$$

The structural problem represented by Eq. (4) is solved with an unsteady, non-linear finite element formulation. The velocities and accelerations are related to the positions through the Wood–Bossak–Zienkiewicz α scheme (Bossak and Zienkiewicz, 1980). The overall motions of the swimmer are unconstrained in translations and rotation and hence thrust production leads to resolved self-propulsion. The structure is discretized using Euler–Bernoulli beam elements with a small deformation, large rotation formulation. The mass matrix is discretized with a direct, diagonal lumped-matrix approach with the mass split between the end beam nodes.

Table 1
Non-damped, modal frequencies of feedback swimmer, embedded in fluid $EI = 30$ N m^2, $m = 100$ kg m^{-1}, $\rho = 1000$ kg m^3.

Mode	F_1	F_2	F_3
Natural frequency (Hz)	1.071	3.126	6.397

While fish are neutrally buoyant, the added mass they are subjected to may be greater than its mass. The added mass is known to be destabilizing to partitioned fluid–structure coupling schemes in which the fluid and structure are solved independently in an iterative manner (Badia et al., 2008). The segregated, quasi-monolithic approach of Durand et al. (2014) is used here; this method can be viewed as a block-LU factorization of the monolithic, coupled system.

Proprioceptive feedback provides a means of correcting for external disturbances and permits modulating the central pattern generator signal. Gazzola et al. proposed a simple feedback signal for applying a bending moment based on the small deflection approximation of the curvature with a delay (Gazzola et al., 2015). In the present work, a feedback model based on this idea is developed. As the elastic beam is completely nonlinear, the true curvature of a cubic spline representation of the swimmer is implemented, unlike in Gazzola et al. The cubic spline representation closely mirrors the shape functions used for the Euler–Bernoulli beam elements. The amplitude of the feedback model bending moment is given as:

$$M_f(s,t) = \chi\kappa(s, t-\tau) \tag{6}$$

where τ is the delay, and χ is the strength of the response to the curvature κ. The cubic spline has N-2 equations for N unknowns. To close the system, two conditions must be imposed. As the swimmer is free, the end feedback bending moments and curvature are imposed to zero at the ends in agreement with the boundary conditions (5). To simplify the temporal scheme, we choose the delay to be a multiple of the time step size Δt. To allow finer variations of feedback delay, we use $\Delta t = 0.00125$ s.

A one meter long swimmer with uniform linear mass of $m = 100$ kg m^{-1} and linear bending stiffness of $EI = 30$ N m^2 is used. This linear mass value has been chosen arbitrarily, although a 2 m long swimmer would weigh more than 100 kg (for example the average mass of a sea lion is 300 kg, while its average length is 2.4 m). In addition, the added mass developed for locomotion is larger that the mass of the swimmers, such that the linear mass value becomes less relevant in locomotion behavior (at least for in cruising motions). The swimmer is discretized with 20 beam elements with 20 co-located fluid elements as shown in Fig. 1. Doubling the panel and element resolution was found to have minimal impact on the predicted swimmer behavior. The swimmer is immersed in idealized water of density $\rho = 1000$ kg m^{-3}. The fluid is inviscid and no viscous drag is directly present. The non-dampened, free natural frequencies of the embedded swimmer are reported in Table 1. These values were computed using modal analysis. We will study the cases of $\eta = 0.005$ s, 0.010 s, 0.020 s. The feedback amplitude χ is constant along the swimmer's length, and we varied it from $\chi = 2.5$ N m rad^{-1} to 7.5 N m rad^{-1}. The swimmer generates pressure drag only if it is oscillating. To assure that non-propulsive states asymptote to zero velocity, an additional drag force equivalent to the viscous drag of Prandtl's turbulent, 1/7 power law boundary layer of a flat plate is added (Schlichting, 1949).

We are interested to understand the influence of feedback delay and damping on the swimming kinematics by measuring the mean forward velocity $\overline{V}$ and the frequency response of the swimmer. The structure is slightly bent to initiate the feedback process. If the feedback is effective in exciting the system, the deformations will grow until an equilibrium is achieved in a self-propulsive state. If the feedback is not destabilizing the structure, the initial perturbation will dampen out and no self-propulsion will be generated. The particle wake method releases a particle at each time step to enforce the unsteady Kutta condition. At the beginning of the computation, the swimmer is immobile and particles would be emitted on top of one another which will lead to the divergence of the fluid solution. To avoid this non-physical effect, the swimmer is given a small initial forward velocity of $V_{initial} = 0.0001$ m s^{-1}. Our numerical code is run until a quasi-steady state is achieved. Frequency domain results are obtained by discrete FFT over 16384 (2^{14}) time steps. We have defined the instantaneous velocity of the swimmer as the average velocity of the 21 nodes. Mean velocities are then found by averaging over the FFT interval.

In Fig. 2, we illustrate a typical swimmer deformation during one period, by representing its spine with the rigid-body translations and rotations removed. The curve exhibits a first mode, but it is not symmetric about the swimmer's mid-length as evident by the $t = \frac{2}{8}T$ and $t = \frac{5}{8}T$ instances compared to the $t = \frac{3}{8}T$ and $t = \frac{7}{8}T$ instances. This is because the fluid load is not symmetrical due the enforcement of the unsteady Kutta condition at the tail on the right end of the swimmer. For self-propulsion to occur, the symmetry of the fluid forces must be broken so that a net force is generated in a sense of travel. Once such a symmetry is broken, the feedback naturally amplifies the asymmetry and thrust is sustained when the delay is in the range of τ that are excitatory. The swimmer experiences an initial transient behavior during which it accelerates before oscillating in its forward velocity as shown in Fig. 2b. These oscillations dampen to a quasi-steady behavior with small oscillations at twice the response frequency. We hypothesize that the typical time scale to reach the steady regime is proportional to the inverse of η. Hence the smaller the damping, the longer will be the transient dynamics.

The hydrodynamic forces acting on the swimmer are generated by the time varying vorticity distribution, which is shown with the wake particles in Fig. 3. The body exhibits a first mode deformation while experiencing a small periodic rigid-body pitching rotation. We remark that the vorticity is distributed into four regions along the body length. Near the head region,

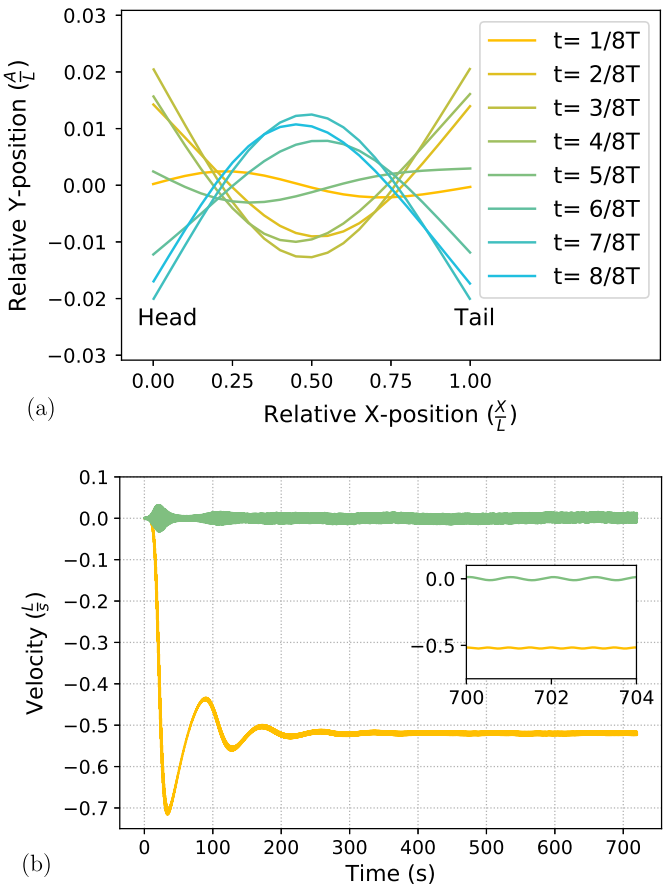

Fig. 2. (a) Deformed swimmer over one period with the head on the left and the rigid-body motions removed. The first free mode is evident, but is not symmetric about its mid-length due to the hydrodynamic loading. (b) Temporal evolution of the swimmer velocities of the mass center; $V_\perp$ (green), is the lateral velocity with respect to the average orientation of the deformed swimmer body while $V_\parallel$ (orange) is the velocity in the sense of the average orientation, whose steady state average is $\overline{V}$. $\eta = 0.005$ s, $\frac{\tau}{I_1} = 0.63$ and $\chi = 7.5$ N m rad^{-1}. The inset in (b) shows the asymptotic dynamics of the two velocities. (For interpretation of the references to color in this figure legend, the reader is referred to the web version of this article.)

the vorticity reflects the flow as it tries to pass around the leading edge due to the head's relative upward transverse motions. A leading edge suction is developed which generates a significant portion of the thrust force. Downstream of the head, the fluid is initially being rotated in a clockwise sense while further aft it is rotating in a counter-clockwise sense. The combined action of these two regions causes the fluid near the mid-length to be pushed downwards, perpendicular to the sense of locomotion; this generates an upward inertial force on the swimmer that slows its downward heave motion. When the maximum deflection has occurred, the circulation weakens and changes signs and the process repeats in the opposite sense. The trailing edge region enforces the Kutta condition and generates the wake. A classic thrust producing reverse von Kármán street is observed downstream.

The use of a delayed curvature feedback leads to a distinct behavior compared with other driving mechanisms. To highlight these differences, we also consider the case of a swimmer with an imposed sinusoidal traveling wave of bending moment:

$$M_{imposed}(s,t) = M_{amp}(s)\sin\left(\frac{2\pi}{\lambda}s - 2\pi f t\right) \tag{7}$$

where M_{amp} is the lengthwise moment amplitude distribution, λ is the wavelength of the wave propagating with frequency f. Here the imposed bending moment amplitude increases linearly from 0.5 N m at the head to 2.5 N m at the tail. The wavelength λ is kept equal to the body length and the frequency f is varied between 0.5 Hz and 7.0 Hz so as to include the first three natural frequencies. Such an imposed wave could be thought of as an input from a central pattern generator. The same structure and damping characteristics are used as for the swimmer with feedback.

To demonstrate the capability of our numerical model, we first compare it against the forced, sinusoidal leading edge heave experiment of Paraz et al. (2014), Paraz (2015) and Paraz et al. (2016) in which a flexible, rectangular sheet is given imposed heave at the leading edge. The experiment mimics a two-dimensional geometry by confining the flow to the width

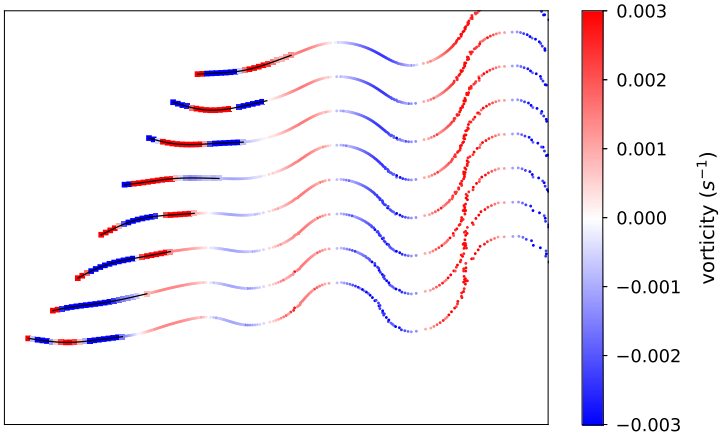

Fig. 3. Vorticity distribution of the swimmer and its wake over approximately one period. $\eta = 0.005$ s, $\frac{\tau}{T_1} = 2.17$ and $\chi = 10$ N m rad^{-1}.

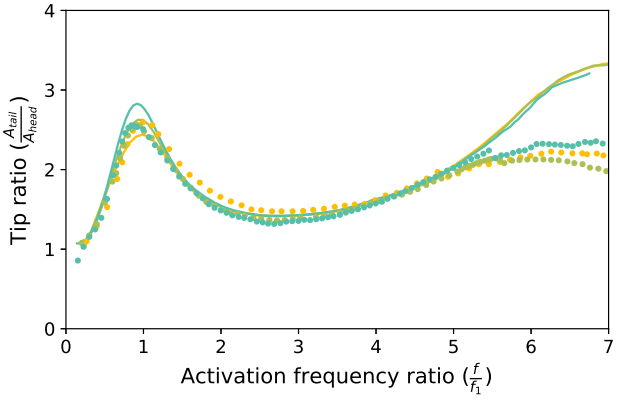

Fig. 4. Tail amplitude response A_{tail} normalized by the imposed head amplitude A_{head} as a function of the ratio of the heave frequency to the first natural frequency for a heave amplitude of $A_{head} = 0.004$ m and Reynolds number of 6000. $EI = 0.018$ (orange), $EI = 0.028$ (green), $EI = 0.053$ (blue). Curves: results of present work. Disks: results of Paraz et al. (2014) . (For interpretation of the references to color in this figure legend, the reader is referred to the web version of this article.)

of the sheet by the walls of the tunnel. Three values for the stiffness, EI $= 0.018,\ 0.028,\ 0.053$ N m are considered at a Reynolds number of 6000 and heave amplitude of $A = 0.004$ m. Further details of the experiment are given in Paraz et al. (2014), Paraz (2015) and Paraz et al. (2016).

3. Results

3.1. Imposed leading edge heave

The behavior of a flexible sheet subjected to imposed leading edge heave is used first to validate the numerical model of the fluid and beam. In the work of Paraz et al. (2014), Paraz (2015) and Paraz et al. (2016), the amplitude and relative phase of the trailing edge were measured over a range of frequencies including the first two natural modes of the sheet. The measured ratio of the trailing edge displacement amplitudes to that of the leading edge is given in Fig. 4. Like in the experiments, a sharp peak in the amplitude appears at the first natural frequency, followed by a wider peak at the second natural frequency. The peak frequencies correspond to the natural frequencies of the sheet, embedded in the fluid. There is closer agreement for the first peak's amplitude, whereas the amplitude of the second peak is overpredicted. In the model (Paraz et al., 2016), the authors included both a linear viscous damping coefficient and a non-linear quadratic damping term to account for the pressure drag induced by the fluid.

In the present case, we did not include a linear viscous damping, while the pressure drag is implicitly present in our model rather than imposed, hence it is not surprising to have an over-prediction of the amplitude. Despite this over-prediction, the good qualitative agreement with the experiments demonstrates the adequacy of the present model.

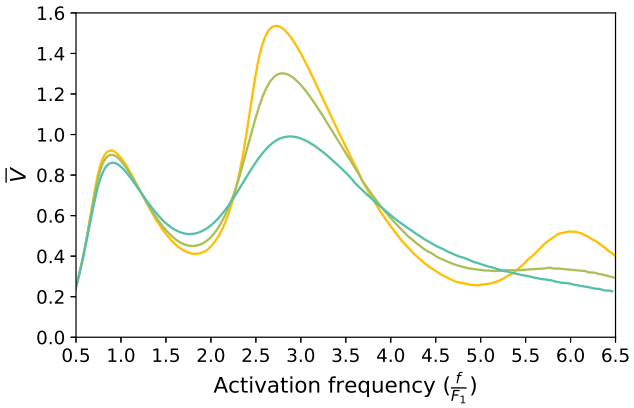

Fig. 5. Mean forward velocity $\overline{V}$ of the imposed bending moment wave as a function of the frequency f normalized by the first natural frequency F_1 for various Kelvin–Voigt damping coefficients. $\eta = 0.005$ s (orange), $\eta = 0.010$ s (green), $\eta = 0.020$ s (red) . (For interpretation of the references to color in this figure legend, the reader is referred to the web version of this article.)

3.2. Imposed traveling wave bending moment

To highlight the distinct self-propulsive characteristics of delayed feedback, we contrast its properties to that of an imposed traveling bending moment wave. Consequently, we study the effect of the imposed moment defined in (7). We first note that the response frequency is always equal to the forcing frequency f. As expected from the leading edge forcing results, the mean velocity $\overline{V}$ of the imposed moment exhibits peaks with respect to the driving frequency, as shown in Fig. 5. The three observed peaks correspond to the first three deformation modes of the swimmer. Such a property arises in swimmers with imposed bending moments (Gazzola et al., 2015) and flexible foils with forced leading edge motions (Paraz et al., 2016; Piñeirua et al., 2017). Similarly to low dimensional driven oscillators, the maximum amplitudes increase as the damping is decreased while the troughs are reduced in depth as the damping increases. As the Kelvin–Voigt model tends to over-damp higher frequencies, the third mode response is absent for $\eta = 0.020$ s. The location of the second peak relative to the first in Fig. 5 differs from that of the foil with imposed leading edge in Fig. 4. This is attributable to both the difference in boundary conditions and the difference in the ratio of bending stiffness to beam mass.

3.3. Feedback delay bending moment

We simulate the dynamics of the swimmer driven by the feedback moment (6). Naturally, we expect the relevant delay value to be linked to a temporal time scale. We associate this time scale to the period T_1 of the first deformation mode. Therefore, the mean forward velocity of the feedback swimmer must depend on η and τ/T_1. The feedback propelled swimmer's response is distinct from that of the imposed traveling wave swimmer. For a given feedback amplitude, our simulated model shows that the normalized delay τ/T_1 needs to be properly selected in order to induce a non-zero forward velocity, see Fig. 6. Six local maximum in the mean velocity are evident over the range of τ/T_1; their width and amplitude decrease as the damping increases. For a delay amplitude of $\chi = 7.5$ N m N m rad^{-1}, we remark that the third peak location is slightly greater than the natural period of the first mode, as $\frac{\tau}{T_1} = 1.15$. Three larger peaks are approximately situated at $\pm 0.5T_1$ from each of the three smaller peaks, and this may be explained with the simple model described in the next section. All six peaks represent amplified responses with a period T close to T_1, as seen in Fig. 7. More precisely, for these six regions, the T/T_1 increases as the ratio τ/T_1 augments. Hence, the feedback swimmer undulates at the first deformation mode. Concerning the influence of the damping coefficient, the variation of the responses period decreases as η grows, because it attenuates the motion away from the peaks. Although, $\eta = 0.02$ s induces a slightly shorter period, for the three larger peaks. Between each pair of peaks is a range of feedback delay ratios for which the swimmer is inefficient in displacing itself, and the response drops very abruptly (for example near $\frac{\tau}{T_1} = 0.85,\ 1.4$).

The effect of the damping is summarized as follows. First, large damping reduces the cruising velocity, which makes sense, since input power is lost into the internal friction. Second, increasing η make smaller the regions of parameters for which the foil swims. Taking the limit of very small damping results in rendering smaller the domains where there is no propulsion. In addition, the unconstrained amplitude growth leads to complex dynamics resulting from the competition between higher mode numbers.

Like the damping, the feedback strength has a strong, nonlinear influence on the swimming speed. Here we vary χ between 2.5 and 7.5 N m rad^{-1} while keeping η fixed as shown in Fig. 6b. For $\chi = 2.5$ N m rad^{-1} the motions are completely damped out and no self-propulsion is achieved. As the feedback amplitude grows, the velocity increases non-linearly as it provides a larger bending moment which in turn elicits an increasing curvature.

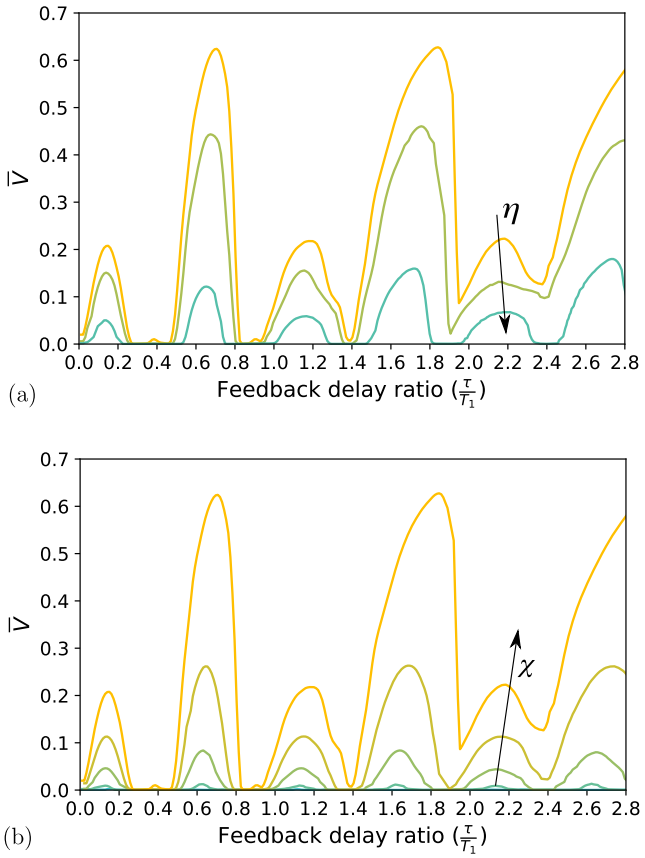

Fig. 6. Mean forward velocity $\overline{V}$ as feedback delay ratio τ/T_1 is varied (a) for different Kelvin–Voigt damping coefficients. $\eta = 0.005$ s (orange), $\eta = 0.010$ s (green), $\eta = 0.020$ s (blue), for $\chi = 7.5$ N m rad^{-1}. (b)as χ is varied $\chi = 3.25$ N m rad^{-1} (blue), $\chi = 5.0$ N m rad^{-1} (green), $\chi = 6.25$ N m rad^{-1} (beige), $\chi = 7.5$ N m rad^{-1} (orange), for $\eta = 0.005$ s . (For interpretation of the references to color in this figure legend, the reader is referred to the web version of this article.)

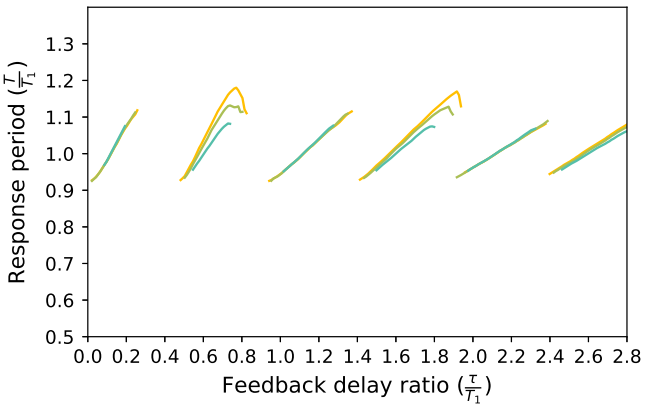

Fig. 7. Oscillation period over first natural period as feedback delay ratio τ/T_1 is varied for different Kelvin–Voigt damping coefficients. $\eta = 0.005$ s (orange), $\eta = 0.010$ s (green), $\eta = 0.020$ s (blue). $\chi = 7.5$ N m rad^{-1} . (For interpretation of the references to color in this figure legend, the reader is referred to the web version of this article.)

3.4. Simplified oscillator model

To explain the appearance of three small peaks with the central peak at a period slightly greater than the natural period and three larger peaks located approximately $\pm 0.5T_1$ from the smaller peaks we consider a simpler representation of the feedback swimmer. As we are concerned with only the first bending mode of the beam, we may approximately reduce the

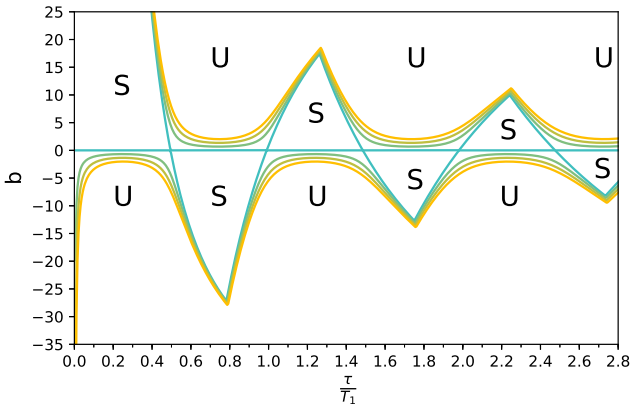

Fig. 8. Marginal stability curves of the delayed damped oscillator when the normalized delay is varied for different amounts of damping. The letter "U" labels unstable regions, while the letter "S" labels stable regions. Blue $\eta\delta = 0.0$, green $\eta\delta = 0.1$, beige $\eta\delta = 0.2$, orange $\eta\delta = 0.3$. (For interpretation of the references to color in this figure legend, the reader is referred to the web version of this article.)

swimmer dynamical equation to that of a damped, delayed, harmonic oscillator, with an equivalent mass, stiffness, and damping. Let us define δ to be the ratio of the effective stiffness to the inertia and b to be the amplitude of the feedback normalized by the inertia. Recalling that the Kelvin–Voigt damping is directly proportional to the stiffness then the damped oscillator equation is:

$$\ddot{y} + \eta\delta\dot{y} + \delta y = by(t - \tau) \tag{8}$$

The reduction of the swimmer beam equation to this low dimensional ODE might be justified by investigating the dynamics of an oscillating mode of the system, in the spirit of Llorens et al. (2016). The stability regions of Eq. (8) may be readily determined using standard techniques (Hu et al., 1998; Driver, 2012).

We numerically computed the instability regions using the semi-discretization method (Insperger and Stépán, 2002, 2003). A stiffness–mass ratio $\delta = 45.3\ \mathrm{s}^{-2}$ is chosen to match the first natural frequency of the swimmer. The marginal stability curves of b as a function of τ are shown in Fig. 8, for different values of $\eta\delta$. Areas bounded by the curves are regions where $y = 0$ is stable while the zones exterior to these boundaries are unstable. We propose to relate the region of stability of the simple model (see Fig. 6) to the observed peaks for the complete swimming model (Fig. 8). The second, fourth and sixth velocity peaks in Fig. 6 correspond to the unstable regions for positive values of b. The three smaller velocity peaks in Fig. 6 corresponds to the unstable zones for the negative values of b : no instability should develop in this regions. This is not what we observe for the complete model for the swimmer. We interpret it as the resonance with harmonics generated by nonlinearities; this simple linear model cannot predict such a phenomena. Increasing the damping leads to smaller unstable regions, similarly to what we observed for the feedback swimmer velocity peaks. The boundaries of the unstable zones are somewhat wider than the peaks in the velocity, as they extend to larger values of τ, but are qualitatively in agreement with the feedback swimmer velocity curves. Each new velocity peak starts at feedback delay ratios that matches when the stable regions for $\eta\delta = 0.0$ changes between positive and negative b.

4. Conclusions

The fluid–structure model of the swimmer was shown to be qualitatively matching with the experimental work of Paraz et al. (2014), Paraz (2015) and Paraz et al. (2016) in which a flexible plate is subjected to forced, leading edge heave. The use of a curvature proportional, time delayed feedback was found to be sufficient to induce self-propulsion in the swimmer. This agrees with the observation of Gazzola et al. (2015) that a central generator is not necessary for a self-propulsive behavior. Nevertheless, the present study reveals that multiple response peaks can occur at the first natural period for delay τ both above and below the period of the first mode; unlike what is reported in Gazzola et al. (2015), where each peak corresponds to a different modal frequency. This is contrasted to an imposed traveling wave bending moment distribution which produces high forward velocities when the activation frequency is equal to one of the natural frequencies; this could be interesting to reduce the effect of flesh viscosity, since the lowest frequencies are less damped than the higher ones.

For the range of delay periods and damping coefficients for which the swimmer maintains a first natural period response, the swimmer's response may be qualitatively described by the much simpler single degree of freedom damped, delayed oscillator. Stability analysis of this oscillator with the natural period matched to T_1 of the swimmer showed that the first and third peaks observed correspond to the points of minimal stability for positive values of feedback coefficient b. The second smaller peak corresponds to the second point of minimal stability for negative values of feedback coefficient b.

The use of proprioceptive feedback permits a decentralized approach to propulsion whereby each propulsive unit acts based only on local information without a central pattern generator input. Proprioceptive feedback may permit to attenuate

or augment the response of a central pattern generator based on the local state along a swimmer's body. Such an approach may be useful for flexible robotic swimmers to improve their performance, particularly in unsteady environments where fluid forces may perturb the swimmer. It is our hope that this contribution will further the goal to better understand real swimmer behavior and in enhancing robotic swimmer performance.

Acknowledgments

The authors acknowledge project funding by the UCA^{JEDI} IDEX grant (ANR-15-IDEX-01), and the support from K-Epsilon.

References

Argentina, M., Mahadevan, L., 2005. Fluid-flow-induced flutter of a flag. Proc. Natl. Acad. Sci. 102 (6), 1829–1834.
Badia, S., Quaini, A., Quarteroni, A., 2008. Splitting methods based on algebraic factorization for fluid-structure interaction. SIAM J. Sci. Comput. 30 (4), 1778–1805.
Bainbridge, R., 1958. The speed of swimming of fish as related to size and to the frequency and amplitude of the tail beat. J. Exp. Biol. 35, 109–133.
Bainbridge, R., 1960. Speed and stamina in three fish. J. Exp. Biol. 37, 129–153.
Banks, H.T., Inman, D., 1991. On damping mechanisms in beams. J. Appl. Mech. 58 (3), 716–723.
Bossak, W., Zienkiewicz, O., 1980. An alpha modification of newmark's method. Internat. J. Numer. Methods Engrg. 15 (10), 1562–1566.
Candelier, F., Boyer, F., Leroyer, A., 2011. Three-dimensional extension of lighthill's large-amplitude elongated-body theory of fish locomotion. J. Fluid Mech. 674, 196–226.
Carling, J., Williams, T.L., Bowtell, G., 1998. Self-propelled anguilliform swimming: simultaneous solution of the two-dimensional navier-stokes equations and newton's laws of motion. J. Exp. Biol. 201 (23), 3143–3166.
Charvet, T., 1992. Resolution Numérique de Problems Lies au Comportement des Voiles de Bateau (Ph.D. thesis), Ecole polytechnique.
Cheng, J.-Y., Pedley, T., Altringham, J., 1998. A continuous dynamic beam model for swimming fish. Philos. Trans. R. Soc. B 353 (1371), 981–997.
Driver, R.D., 2012. Ordinary and Delay Differential Equations, Vol. 20. Springer Science & Business Media.
Durand, M., Leroyer, A., Lothode, C., Hauville, F., Visonneau, M., Floch, R., Guillaume, L., 2014. Fsi investigation on stability of downwind sails with an automatic dynamic trimming. Ocean Eng. 90, 129–139.
Ekeberg, O., Grillner, S., Lansner, A., 1995. The neural control of fish swimming studied through numerical simulations. Adapt. Behav. 3 (4), 363–384.
Eldred, L.B., Baker, W.P., Palazotto, A.N., 1995. Kelvin-voigt versus fractional derivative model as constitutive relations for viscoelastic materials. AIAA J. 33 (3), 547–550.
Eloy, C., Doare, O., Ducheemin, L., Schouveiler, L., 2010. A unified introduction to fluid mechanics of flying and swimming at high reynolds number. Exp. Mech. 50, 1361–1366.
Felippa, C.A., Haugen, B., 2005. A unified formulation of small-strain corotational finite elements: I. theory. Comput. Methods Appl. Mech. Engrg. 194 (21–24), 2285–2335.
Gazzola, M., Argentina, M., Mahadevan, L., 2014. Scaling macroscopic aquatic locomotion. Nat. Phys. 112 (10), 758–761.
Gazzola, M., Argentina, M., Mahadevan, L., 2015. Gait and speed selection in slender inertial swimmers. Proc. Natl. Acad. Sci. 112 (13), 3874–3879.
Guan, L., Kiemel, T., Cohen, A.H., 2001. Impact of movement and movement-related feedback on the lamprey central pattern generator for locomotion. J. Exp. Biol. 204 (13), 2361–2370.
Hauville, F., 1996. Optimisation des Méthodes de Calculs Découlements Tourbillonnaires Instationnaires (Ph.D. thesis), Université du Havre.
Hill, A., 1938. The heat of shortening and the dynamic constants of muscle. Proc. Roy. Soc. Lond. B Biol. Sci. 126 (843), 136–195. http://dx.doi.org/10.1098/rspb.1938.0050.
Hu, H., Dowell, E.H., Virgin, L.N., 1998. Resonances of a harmonically forced duffing oscillator with time delay state feedback. Nonlinear Dynam. 15 (4), 311–327.
Huberson, S., 1984. Calcul d'écoulements tridimensionnels instationnaires incompressibles par une méthode particulaire. J. Méc. Théor. Appl. 3 (5), 805–819.
Huberson, S., 1986. Modélisation Asymptotique et Simulation Numérique d'écoulements Tourbillonnaires (Ph.D. thesis), Paris, p. 6.
Insperger, T., Stépán, G., 2002. Semi-discretization method for delayed systems. Int. J. Numer. Methods Eng. 55 (5), 503–518.
Insperger, T., Stépán, G., 2003. Stability of the damped mathieu equation with time delay. J. Dyn. Syst. Meas. Control 125 (2), 166–171.
Katz, J., Plotkin, A., 2001. Low-Speed Aerodynamics. In: Cambridge Aerospace Series, Cambridge University Press.
Leroyer, A., Visonneau, M., 2005. Numerical methods for ranse simulations of a self-propelled fish-like body. J. Fluids Struct. 20 (7), 975–991.
Liao, J.C., Beal, D.N., Lauder, G.V., Triantafyllou, M.S., 2003. The kármán gait: novel body kinematics of rainbow trout swimming in a vortex street. J. Exp. Biol. 206 (6), 1059–1073. http://dx.doi.org/10.1242/jeb.00209.
Lighthill, M., 1960. Note on the swimming of slender fish. J. Fluid Mech. 9, 305–317.
Lighthill, M., 1971. Large-amplitude elongated-body theory of fish locomotion. Proc. Roy. Soc. Lond. Ser. B Biol. Sci. 179 (1055), 125–138.
Llorens, C., Argentina, M., Rojas, N., Westbrook, J., Dumais, J., Noblin, X., 2016. The fern cavitation catapult: mechanism and design principles. J. R. Soc. Interface 13 (114), 20150930.
Melli, J.B., 2008. A Hierarchy of Models for the Control of Fish-like Locomotion (Ph.D. thesis), Princeton University.
Munk, M.M., 1924. The aerodynamic forces on airship hulls, naca report 184, Tech. rep., Washington: NACA.
Pan, V., Reif, J., 1985. Efficient parallel solution of linear systems, Tech. rep., Harvard University.
Pan, V., Schreiber, R., 1990. An improved newton iteration for the generalized inverse of a matrix with applications, Tech. rep., NASA Ames Research Center.
Paraz, F., 2015. Oscillation d'une Plaque Flexible Dans un Écoulement (Ph.D. thesis), Aix Marseille Université.
Paraz, F., Eloy, C., Schouveiler, L., 2014. Experimental study of the response of a flexible plate to a harmonic forcing in a flow. C. R. Méc. 342 (9), 532–538.
Paraz, F., Schouveiler, L., Eloy, C., 2016. Thrust generation by a heaving flexible foil: Resonance, nonlinearities, and optimality. Phys. Fluids 28 (1), 011903.
Piñeirua, M., Thiria, B., Godoy-Diana, R., 2017. Modelling of an actuated elastic swimmer. J. Fluid Mech. 829, 731–750.
van Rees, W.M., Gazzola, M., Koumoutsakos, P., 2013. Optimal shapes for anguilliform swimmers at intermediate reynolds numbers. J. Fluid Mech. 722.
Rehbach, C., 1973. Calcul d'écoulements autour dailes sans epaisseur avec nappes tourbillonnaires evolutives. Rech. Aérospatiale 2, 53–61.
Rehbach, C., 1978. Numerical calculation of three-dimensional unsteady flows with vortex sheets. In: 16th Aerospace Sciences Meeting. p. 111.
Schlichting, H., 1949. Boundary layer theory part ii - turbulent flows, naca report 1218, Tech. rep., Washington: NACA.
Shadmehr, R., Wise, S.P., 2005. The Computational Neurobiology of Reaching and Pointing: A Foundation for Motor Learning. MIT press.
Timoshenko, S.P., Woinowsky-Krieger, S., 1959. Theory of Plates and Shells. McGraw-hill.
Triantafyllou, M.S., Hover, F.S., Techet, A.H., Yue, D.K., 2005. Review of hydrodynamic scaling laws in aquatic locomotion and fishlike swimming. Appl. Mech. Rev. 58 (4), 226–237.
Triantafyllou, G.S., S., T.M., Grosenbaugh, M., 1993. Optimal thrust development in oscillating foils with application to fish propulsion. J. Fluids Struct. 7 (2), 205–224.

Triantafyllou, M.S., Triantafyllou, G.S., Gopalkrishnan, R., 1991. Wake mechanics for thrust generation in oscillating foils. Phys. Fluids A 3 (12), 2835–2837.
Tytell, E.D., Hsu, C.-Y., Williams, T.L., Cohen, A.H., Fauci, L.J., 2010. Interactions between internal forces, body stiffness, and fluid environment in a neuromechanical model of lamprey swimming. Proc. Natl. Acad. Sci. 107 (46), 19832–19837.
Wardle, C., Videler, J., Altringham, J., 1995. Review tuning in to fish swimming waves: body form, swimming mode and muscle function. J. Exp. Biol. 198, 1629–1636.
Webb, P., Kostecki, P., Stevens, E., 1984. The effect of size and swimming speed on locomotor kinematics of rainbow trout. J. Exp. Biol. 109, 77–95.
Willis, D., 2006. An Unsteady, Accelerated, High Order Panel Method with Vortex Particle Wakes (Ph.D. thesis), Massachusetts Institute of Technology.
Wu, T.Y., 1961. Swimming of a waving plate. J. Fluid Mech. 10 (3), 321–344. http://dx.doi.org/10.1017/S0022112061000949.
Wu, T.Y., 2007. A nonlinear theory for a flexible unsteady wing. J. Eng. Math. 58, 279–287.
Yu, Z., Eloy, C., 2018. Extension of lighthill's slender-body theory to moderate aspect ratios. J. Fluids Struct. 76, 84–94.